*35th EPS Conference on Plasma Phys. Hersonissos, 9 - 13 June 2008 ECA Vol.**32D**, P-4.025 (2008)*

Energy and momentum transport induced by unstable ITG modes

M.C. Varischetti, M. Lontano, E. Lazzaro

Istituto di Fisica del Plasma, D.E.T.-C.N.R., EUR-ENEA-CNR Ass., Milan, Italy

Abstract

The quasi-linear equations for the ion pressure and field-aligned momentum are integrated across a plasma slab for initial density, temperature and flow-velocity profiles typical of tokamak experiments, and the energy and momentum diffusivities (χ_E and χ_U, respectively) are calculated during the plasma evolution. The behavior of the Prandtl number $Pr=\chi_E/\chi_U$ is monitored during the injection of auxiliary power and/or momentum, and it turns out that its value stays below 0.5, for a broad range of physical parameter values.

Introduction

The correlation between energy and angular momentum transport observed in different tokamak experiments [1], and the occurrence of an intrinsic toroidal plasma rotation with characteristics that depend on the confinement regimes [2] suggest a common anomalous origin of energy and angular momentum diffusion that can be triggered by unstable ITG modes. In this connection, the drift fluid equations for the ion pressure and parallel flow-velocity, containing the corresponding quasi-linear (QL) fluxes produced by the presence of a **k**-spectrum of unstable ITG modes, with $k_\perp \rho_{Li} < 1$ and $k_\parallel << k_\perp$, have been integrated across a plasma slab in the presence of localized energy and/or momentum sources. The effective diffusivities of ion energy χ_E and parallel momentum χ_U are calculated in the course of the plasma evolution, in different physical conditions and for plasma parameters relevant to different tokamak discharges. It turns out that the Prandtl number $Pr=\chi_U/\chi_E$ tends to remain below 0.5. A momentum influx at plasma edges can cause $Pr > 1$.

The transport equations and the quasi-linear fluxes

Consider a plasma slab (-a<x<+a) with the equilibrium magnetic field laying in the (y,z) plane and depending on the slab coordinate x, as all the other equilibrium physical parameters, like ion density, flow-velocity and pressure. Due to the slowness of the motions we are interested in ($\omega << \Omega_{ci}$), electrons follow a Boltzmann distribution and quasi-neutrality holds. The spatial variation of the magnetic field and its curvature are taken into account by means of a suitable drift velocity [3]. The dependent variable $A(\mathbf{r},t)$ is written in the form of $A(\mathbf{r},t) = \overline{A}(x,t) + \tilde{A}(\mathbf{r},t)$, where $|\tilde{A}(\mathbf{r},t)| << |\overline{A}(x,t)|$, and $\overline{A}(x,t)$ and $\tilde{A}(\mathbf{r},t)$

represent the slowly varying (over length $L_{y(z)}$ and time T) and the rapidly fluctuating (over $\lambda_{y(z)} = 2\pi/k_{y(z)} << L_{y(z)}$ and $\tau = 2\pi/\omega << T$) parts of $A(\mathbf{r},t)$, respectively. Moreover, the properties $\langle A(\mathbf{r},t)\rangle_{y,z} = \overline{A}(x,t)$ and $\langle \tilde{a}(\mathbf{r},t)\rangle_{y,z} = 0$ hold, where the symbol $\langle \bullet \rangle_{y,z}$ indicates spatial averages over the lengths $\ell_{y(z)}$, such that $\lambda_{y(z)} << \ell_{y(z)} << L_{y(z)}$. Then, the QL ion momentum and pressure fluxes in *x* are calculated as spatial averages of the products of the advective drift velocity, $\tilde{v}_{Ex} = -\frac{c}{B}\frac{\partial \tilde{\phi}}{\partial y}$, times the advected fluctuating $\tilde{v}_z$ and $\tilde{p}_i$, that is

$$\Gamma^{\perp}_{v_z}(x,t) = \langle \tilde{v}_{Ex}\tilde{v}_z\rangle_{y,z} = \lim_{\ell_y,\ell_z\to\infty}\frac{1}{\ell_y\ell_z}\int_{-\ell_y/2}^{+\ell_y/2}dy\int_{-\ell_z/2}^{+\ell_z/2}dz\,\tilde{v}_{Ex}\tilde{v}_z = \lim_{\ell_y,\ell_z\to\infty}\frac{1}{\ell_y\ell_z}\int_{-\infty}^{+\infty}dk_y\int_{-\infty}^{+\infty}dk_z\,\tilde{v}_{E,\mathbf{k}}\tilde{v}^{*}_{z,\mathbf{k}}$$

$$\Gamma^{\perp}_{p_i}(x,t) = \langle \tilde{v}_{Ex}\tilde{p}_i\rangle_{y,z} = \lim_{\ell_y,\ell_z\to\infty}\frac{1}{\ell_y\ell_z}\int_{-\ell_y/2}^{+\ell_y/2}dy\int_{-\ell_z/2}^{+\ell_z/2}dz\,\tilde{v}_{Ex}\tilde{p}_i = \lim_{\ell_y,\ell_z\to\infty}\frac{1}{\ell_y\ell_z}\int_{-\infty}^{+\infty}dk_y\int_{-\infty}^{+\infty}dk_z\,\tilde{v}_{E,\mathbf{k}}\tilde{p}^{*}_{i,\mathbf{k}},$$

where the last equalities come from the Parseval identity. These fluxes enter the evolution equations for the regular parts of the ion flow-velocity $\overline{V}_z(x,t)$ and pressure $\overline{P}_i(x,t)$, that is

$$\frac{\partial \overline{V}_z}{\partial t} + \frac{\partial \Gamma^{\perp}_{v_z}}{\partial x} = -\langle \tilde{v}_x\tilde{v}_{y'}\rangle\frac{d\vartheta}{dx} + \frac{1}{M\overline{n}_i^2}\left\langle \tilde{n}_i\frac{\partial \tilde{p}_i}{\partial z'}\right\rangle_{y,z} + \frac{1}{M\overline{n}_i^2}\left\langle \tilde{n}_i\hat{\mathbf{b}}\cdot\left(\nabla\cdot\tilde{\overline{\overline{\Pi}}}\right)\right\rangle_{y,z} + S_{U_z}, \qquad (1)$$

$$\frac{\partial \overline{P}_i}{\partial t} + \frac{\partial \Gamma^{\perp}_{p_i}}{\partial x} = (\gamma-1)\left\langle \tilde{v}_{\parallel}\frac{\partial \tilde{p}_i}{\partial z'}\right\rangle_{y,z} + S_{P_i}. \qquad (2)$$

In the frame of our collisionless model, the QL density flux is zero and $\overline{n}_i(x) = \text{const}$. The RHS of Eqs.(1,2) contains averaged terms, quadratic in the fluctuating potential, which cannot be written as divergence of a flux, and source terms $S_{P_i(U_z)}$. In particular, the first term in the RHS of Eq.(1), proportional to the *x*-derivative of the pitch angle of the magnetic lines of force $\vartheta(x)$, represents the effect of magnetic shear. In the following analysis, different kinds of sources have been considered, while the averaged terms in the RHS have been discarded. The linearized equations for the Fourier coefficients $\tilde{v}_{z,\mathbf{k}}$ and $\tilde{p}_{i,\mathbf{k}}$ allow one to express the quadratic forms to be integrated in k_y and k_z in the QL fluxes as proportional to $\left|\tilde{\phi}_{\mathbf{k}}\right|^2$ [3]. Finally, in order to solve Eqs.(1,2), the saturation level of the modes is determined qualitatively by the "mixing-length" criterion [4]. During the integration, the effective energy and momentum diffusivities, $\chi_i = \Gamma^{\perp}_{p_i}/(\nabla_x\overline{P}_i)$ and $\chi_{v_z} = \Gamma^{\perp}_{v_z}/(\nabla_x\overline{U}_z)$ respectively, are calculated together with the Prandtl number, $Pr = \chi_{v_z}/\chi_i$. Several cases of externally driven plasmas have been investigated, with energy and momentum deposition (S_P, S_{Uz}, respectively) inside the slab or with a momentum source localized at the edge. Also

different boundary conditions have been taken into account: constant boundary values for T_i and U_z or constant (zero) pressure and momentum fluxes at the plasma edges. An energy source S_{P_i} on-axis (and the corresponding S_{V_z}) with peak value ≈ 2MW/m^3 is considered.

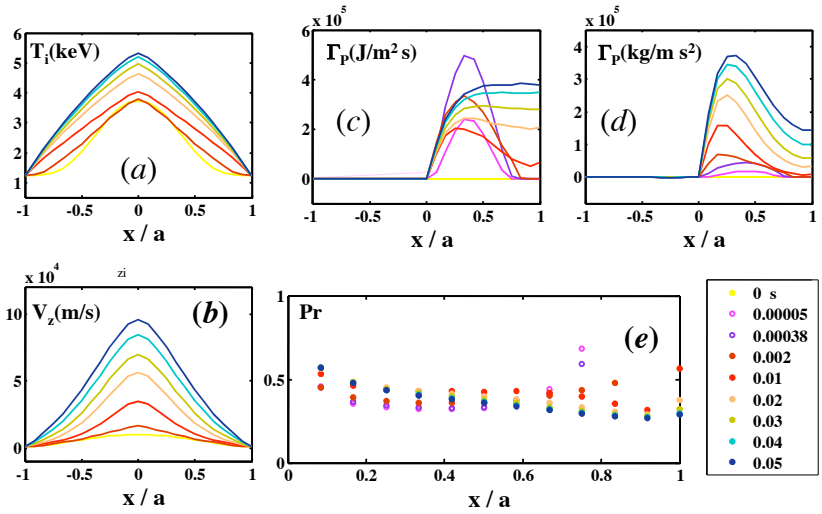

Fig.1

In Fig.1 the spatial profiles (in ξ=x/a) of T_i (*a*), U_z (*b*), $\chi^{\Gamma}_{p_i}$ (*c*), $\chi^{\Gamma}_{v_z}$ (*d*), and *Pr* (*e*) taken at different times (up to t = 0.05 s), in the presence of source terms S_P and S_{Uz} localized on axis, are displayed. Here, the edge values of T_i and of U_z have been kept constant. It is seen that in the confinement region, 0.2<ξ<0.8, 0.4<*Pr*<0.5, but during the initial transient.

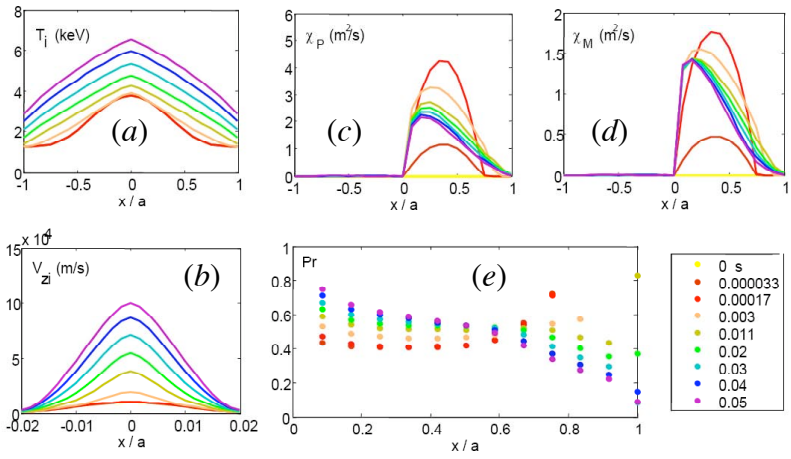

Fig.2

In Fig.2, T_i (*a*), U_z (*b*), χ_i (*c*), χ_{Vz} (*d*), and *Pr* (*e*) *versus* ξ are shown for zero fluxes at ξ=±1, simulating the presence of an edge transport barrier. Here, in the range 0.4<ξ<0.6, *Pr* is around 0.5, having elsewhere a wider spread than in Fig.1*e*.

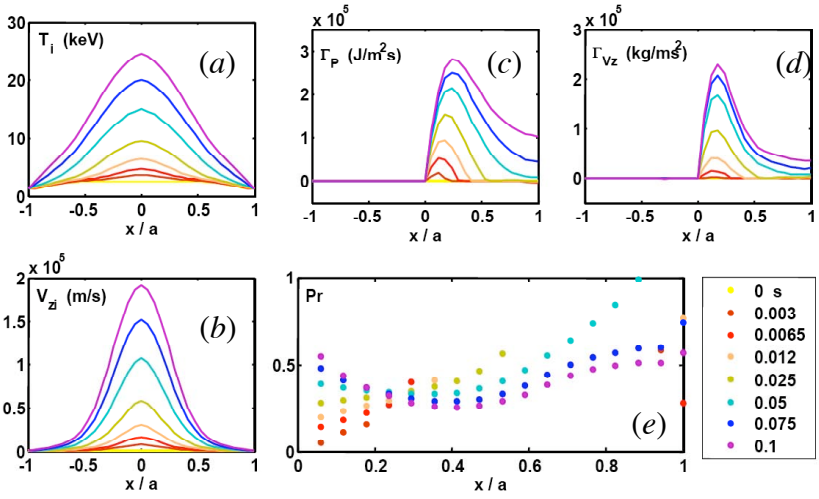

Fig.3

In Fig.3, the same quantities as in Fig.1 are shown for a JET-like case. It is seen that, although the physical parameters are quite different from those considered in the previous cases, 0.4<*Pr*<0.5 in the region between 0.2 and 0.8. A common feature of the plots (e) is that in the LFS part of the slab, *i.e.* for 0<ξ<1, the value of *Pr* tends to increase close to the origin and to decrease in the outer region, remaining almost constant around mid radius.

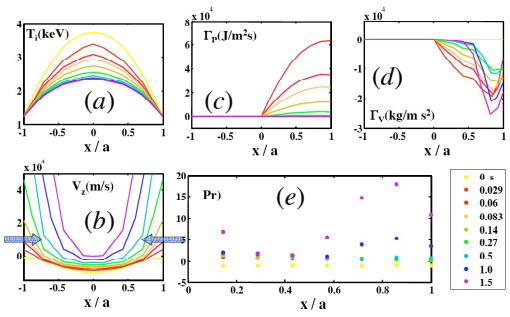

Fig.4

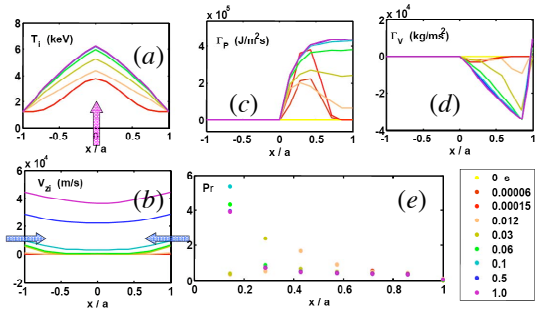

Fig.5

In Figs.4,5 the interplay of momentum and energy sources is shown. In both AUG-like plasmas (same plots as in Fig.1), a momentum source is applied to the plasma edges (horizontal blue arrows) while an on-axis energy source (vertical pink arrow) acts on the plasma of Fig.5, only. The comparison of the two plots (*b*) shows that the inward diffusion of momentum is inhibited by the decreasing T_i (left plot), while the heated plasma (right) favors momentum transport. In addition, plots (*e*) show that in the presence of a momentum influx at the edges, *Pr* can achieve relatively high values.

1 – T. Tala, *et al.*, *Plasma Phys. Contr. Fus.* **49**, B291 (2007).
2 – J.E. Rice, *et al.*, *Nucl. Fus.* **47**, 1618 (2007).
3 –M. Lontano, et al., Proc. *Joint Varenna-Lausanne Int. Workshop on Theory of Fusion Plasmas*, Varenna, Aug.28-Sept.1, 2006, edited by J. Connor et al., AIP Conference Proceedings #**871**, p.374, 2006; J.R. Myra, *et al.*, *21st IAEA Fusion Energy Conference*, Oct. 16-21, 2006, Chengdu, China
4 – M.C. Varischetti, *et al*, *34th EPS Conf. On Plasma Phys.*, Warsaw, 2007, ECA Vol.**31F**, P-4.048 (2007).